

Silica-Based Infiltrations for Enhanced Zirconia-Resin Interface Toughness

N.C. Ramos^{1,2} , M.R. Kaizer² , T.M.B. Campos³, J. Kim⁴, Y. Zhang² ,
and R.M. Melo¹

Abstract

Novel silica-based infiltrations on the surface of zirconia have the potential to improve their bondability, allowing for the etching/silane adhesive bonding technique. Nonetheless, adhesively bonded joints are subject to mixed tensile and shear stresses when the restoration is in occlusal service. Thus, we aimed to investigate the effect of 2 novel silica-based infiltrations on the interfacial toughness of adhesively bonded zirconia using the Brazil nut method, which allows for controlled types of stresses to be applied at the interfaces. In total, 150 3Y-TZP (In-Ceram YZ; Vita) Brazil nuts were machined and randomly assigned to 3 groups: C, control (air abraded); SG, sol-gel silica infiltration; and GI, glass infiltration. SG specimens were immersed twice in silicic acid for 20 min and dried (100°C, 1 h). GI specimens were presintered (1,400°C, 1 h) before a glass powder slurry was applied to the intaglio surface. All specimens were then sintered (1,530°C, 2 h). Following adhesive bonding (Panavia F 2.0, Kuraray) and water storage (37°C) for 10 d, the Brazil nuts were subdivided into groups baseline and aged (40,000 thermal cycles between 5°C and 55°C, with a dwell time of 30 s). The Brazil nuts were subjected to axial-loading tests using various inclinations (precrack angle with load direction): $\Theta = 0^\circ, 5^\circ, 10^\circ, 15^\circ, \text{ or } 25^\circ$, which define the stress type at the interface, from pure tension (0°) to increasing levels of shear. Under pure tension (0°), GI yielded superior interfacial fracture energy, SG and C were similar, and aging had no effect. Under predominantly shear stresses (25°), aging significantly decreased interfacial fracture energy of C and SG, while GI remained stable and was superior. The glass infiltration of the zirconia intaglio surface increases its adhesive bonding interfacial toughness. The sol-gel silica infiltration method requires improvement to obtain a homogeneous surface infiltration and an enhanced bond strength.

Keywords: ceramics, resin cements, bonding force, fracture strength, tensile strength, shear strength

Introduction

Dental zirconias have excellent mechanical properties, but achieving adequate adhesive bonding is still challenging. Several studies have been published over the years aiming to modify zirconia surface chemistry and improve its bondability. That is the case of the graded zirconia proposed by Yu Zhang and collaborators (Zhang and Kim 2009; Zhang and Ma 2009). The graded zirconia is obtained by glass infiltration on the zirconia surface, resulting in a transient composition from a glass-rich surface followed by a glass/zirconia graded layer, where the glass percentage gradually decreases in depth toward a dense zirconia core. According to Zhang's findings (Zhang and Kim 2009; Zhang and Ma 2009; Kim et al. 2010; Zhang and Kim 2010; Zhang 2012; Zhang et al. 2012), glass-infiltrated zirconia is more esthetic than homogeneous zirconia. It is also stronger than porcelain-veneered zirconia due to greater resistance to fracture and chipping, since the glass is diffused into the zirconia surface, which, in turn, transfers stresses into the subsurface. In addition, the glass-rich surface can be acid etched and silanized, resulting in a strong and stable adhesive bond (Chai et al. 2015).

Various methods to promote silica-based deposition or infiltration on inert ceramics have been proposed, aiming to allow for silane-adhesive bonding (Vanderlei et al. 2014; Oliveira-Ogliari et al. 2015; Samodurova et al. 2015; Campos et al.

2016; Kaizer et al. 2016). A novel method has been recently proposed for the infiltration of zirconia with silica by using a sol-gel technique (Campos et al. 2016). The authors reported the successful silica infiltration within the zirconia microstructure, resulting in a silica-rich infiltrated layer of $\sim 6 \mu\text{m}$ in depth (Toyama et al. 2019). Thus, no interference with the internal fit of the silica-infiltrated restoration is expected. This technique

¹Department of Dental Materials and Prosthodontics, Institute of Science and Technology of São José dos Campos, São Paulo State University (UNESP), São José dos Campos, SP, Brazil

²Department of Biomaterials and Biomimetics, New York University College of Dentistry, New York, NY, USA

³Department of Physics, Aeronautical Technology Institute (ITA), São José dos Campos, SP, Brazil

⁴Department of Civil and Environmental Engineering, University of Connecticut, Storrs, CT, USA

Corresponding Authors:

R.M. Melo, Department of Dental Materials and Prosthodontics, Institute of Science and Technology of São José dos Campos, São Paulo State University (UNESP), 777 Eng. Francisco Jose Longo Avenue, São José dos Campos, SP 12245-000, Brazil.
Email: renata.marinho@unesp.br

Y. Zhang, Department of Biomaterials and Biomimetics, New York University College of Dentistry, 433 First Avenue, Room 810, New York, NY 10010, USA.
Email: yz21@nyu.edu

does not require complex equipment, and the results of Campos et al. (2016) showed better structural homogeneity and better bond strength compared to homogeneous zirconia, while the mechanical properties remain similar. Another potential advantage of silica-based infiltrations in zirconia is preventing its exposure to the oral environment and avoiding low-temperature degradation (Chevalier et al. 2009).

The interfacial fracture toughness is an inherent property that measures the resistance of a given interface to crack propagation. The double cantilever beam (DCB) and notchless triangular prism specimen (NTP) are possible methodologies that use specimen geometry easy to produce, and the fracture energy is not dependent on cement thickness. However, these test methods only measure interfacial fracture toughness under tensile loading (Chai et al. 2015; Mesmar and Ruse 2017). In contrast, the Brazil nut specimen geometry allows for the measurement of interfacial fracture toughness in the complete range of failure modes (Wang and Suo 1990; Zhou et al. 2006; Melo et al. 2011): when the interface is positioned axially with the loading direction (0°), the interface experiences pure tensile stresses and fractures in mode I. On the other hand, the angulation of the interface with respect to loading direction produces increasing shear stresses with increasing angles (mixed-mode fractures). Finally, at a given inclination angle, which is a function of interface and precrack sizes, fracture occurs due to pure shear stresses (mode II). This is the only interfacial fracture toughness test method that simulates the variations of the mixed stress modes occurring in occlusal loading in an oral cavity (Zhou et al. 2006; Melo et al. 2011; Mesmar and Ruse 2017).

The objective of this study was to evaluate the interfacial toughness of the adhesive bonding between the zirconia and resin cement from the point of view of linear elastic fracture mechanics using Brazil nut specimens. To compare the interfacial energies (fracture toughness) of the bonded resin cement and zirconia, air abraded zirconia was used as reference, and 2 silica infiltrations were prepared by using either the sol-gel or the glass infiltration (graded zirconia) method. The null hypothesis tested was that both silica-based infiltrations and conventional zirconia would present similar behavior.

Materials and Methods

Specimen Preparation

Zirconia blocks (Vita InCeram YZ; Vita Zahnfabrik) were soft-machined in the shape of the Brazil nut specimens (Fig. 1). The final diameter of the Brazil nut was $2R = 10$ mm, and its thickness was $t = 5$ mm. The elliptical internal defect length (precrack) was $2a = 1.5$ mm. The specimens were randomly assigned to 3 groups according to surface treatment ($n = 50$): C, control group (zirconia as machined); SG, sol-gel group (infiltration with silicic acid— $\text{Si}(\text{OH})_4$); and GI, glass-infiltrated zirconia (infiltration with an in-house silica-based glass).

For the sol-gel method, $\text{Si}(\text{OH})_4$, or silica sol, was obtained from hydrated sodium metasilicate ($\text{Na}_2\text{SiO}_3 \cdot 5\text{H}_2\text{O}$), following the same procedures described by Campos et al. (2016).

However, a basic catalyst (ammonium carbonate) was added at a concentration of 1 g per 100 mL of $\text{Si}(\text{OH})_4$ solution to reduce the infiltration time due to a pH increase from 2 to 7 (Brinker 1988). Specimens were immersed twice in silicic acid for 20 min and dried (100°C , 1 h) prior to sintering.

For the glass infiltration, the protocol developed by Zhang and Kim (2009) was used. The green-body Brazil nuts were presintered at $1,400^\circ\text{C}$ for 1 h to reach ~95% density. An in-house developed silicate glass slurry (SiO_2 [65.5%], Al_2O_3 [11.7%], K_2O [10.0%], Na_2O [7.3%], CaO [3.0%], and Tb_4O_7 [1.9%]) was brushed onto the intaglio surfaces of the Brazil nuts, and then infiltration happened along with sintering. The glass composition had been specifically developed to yield a similar coefficient of thermal expansion to that of zirconia.

For the C group, specimens were sintered as machined. Specimens from all groups were sintered according to the zirconia manufacturer instructions at $1,530^\circ\text{C}$ for 2 h. After sintering, the specimens were cleaned using an alcohol ultrasonic bath for 2 min, followed by a distilled water ultrasonic bath for 2 min.

For adhesive bonding, the intaglio surface of the C group was air abraded with $50 \mu\text{m}$ aluminum oxide particles at 0.2 MPa pressure, at a 1-cm stand-off distance (Micro etcher). For the SG group, the intaglio surface was etched with hydrofluoric acid 2% for 10 s (Campos et al. 2016), and for the GI group, the intaglio surface was etched with hydrofluoric acid 5% for 5 min. After surface treatment, the specimens were cleaned using a distilled water ultrasonic bath for 2 min and dried. The resin bonding system used in this study was Panavia F 2.0 (Kuraray Noritake Dental), and the instructions from the manufacturer were followed: K etchant was applied on the intaglio surface for 5 s, washed, and dried; Clearfil Ceramic Primer was then applied and left undisturbed for 2 min. The resin cement Panavia F 2.0 was mixed and immediately applied to one of the halves of a Brazil nut specimen, and then a cementation jig was used to bond the 2 halves of the specimens. The resin-based Panavia bonding systems are considered gold standard for zirconia adhesive bonding. The successful clinical findings (Kern et al. 2017) are attributed to the presence of MDP (10-methacryloyloxydecyl dihydrogen phosphate), a molecule proven to bond to the zirconia surface (Tanaka et al. 2008; Kern 2015).

The specimens were stored in distilled water at 37°C for 10 d for complete hydration and polymerization of the resin bonding agent. The specimens were then randomly allocated into baseline and aged groups. The baseline groups were tested immediately, and the aged groups were placed in a thermocycling machine with water baths at 5°C and 55°C (with 30-s dwell time each) for 40,000 cycles (~4 mo) and then tested.

Fracture Energy Test (G)

The interfacial fracture tests were conducted on a universal testing machine equipped with a load cell of 10 kN (Instron 5566). Brazil nut specimens were loaded with a 0.03-mm/min travel speed. The precrack was positioned at different angles (Θ) relative to the load direction (Fig. 1C). For each surface

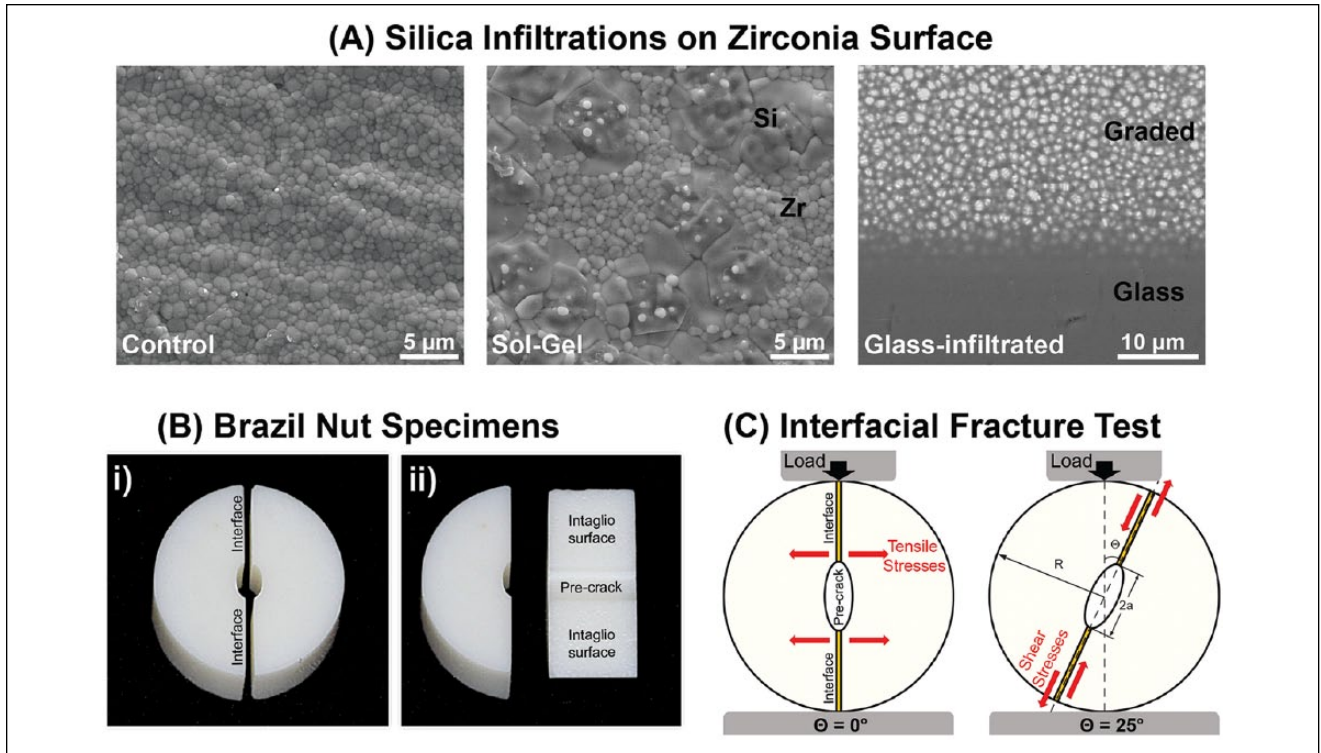


Figure 1. Description of the study design: **(A)** Scanning electron microscopy images showing the microstructure of the zirconia used in this study, from left to right; as machined (InCeram YZ), the sol-gel-treated zirconia (surface view) with silica islands intermingled within zirconia grains and the glass-infiltrated zirconia, which was polished in a shallow angle to expose the underlying zirconia/glass graded layer. **(B)** Digital photograph of a Brazil nut specimen: i) side view of the 2 halves and ii) detail of the intaglio surface and precrack on one of the halves. **(C)** Schematic of the load-to-fracture test setup, where $2a$ is the crack length, R is the radius of the Brazil nut specimen, and Θ is the angle between the loading direction and crack orientation. At $\Theta = 0^\circ$ and $\Theta = 25^\circ$, illustration of the direction of stresses applied to the bonded interface is shown.

treatment, 5 specimens were tested using each precrack angle ($\Theta = 0^\circ, 5^\circ, 10^\circ, 15^\circ,$ or 25°) at baseline and after aging. The maximum load P at the interfacial fracture was recorded, which was then used to calculate the energy release rate, G_c .

When an axial load P is applied to a Brazil nut, the crack is subjected to tensile mode I, shear mode II, or a combination of both stresses according to the precrack angle (Wang and Suo 1990) and shape. For a homogeneous Brazil nut specimen (as shown in Fig. 1C but without an interfacial layer), the stress intensity factors corresponding to mode I (K_I) and mode II (K_{II}) can be derived by fitting polynomial forms (Atkinson et al. 1982) using the precrack angle Θ , critical load P for interfacial fracture, and relative precrack length a/R , where $2a$ is the precrack length and R is the radius of the Brazil nut (Fig. 1C).

The combination of modes I and II is characterized by the load phase Ψ , which is controlled by the precrack angle Θ . The specimen is under pure tensile stress when $\Theta \approx 0^\circ$ and predominantly shear stress when $\Theta \approx 25^\circ$. The loading phase is calculated by equation (1):

$$\Psi = \tan^{-1} \left(\frac{K_{II}}{K_I} \right). \quad (1)$$

The critical condition for the crack growth is given by the energy release rate G_c (N/m), so that the interface debonds. This is given by equation (2):

$$Gc = G_1 + G_2 = \frac{1}{E_1} (K_I^2 + K_{II}^2), \quad (2)$$

where G_1 and G_2 are the energy release rates of modes I and II, respectively, and E_1 is Young's modulus in the plane strain state.

Failure Patterns Characterization

After the interfacial fracture test, all of the specimens were evaluated using stereomicroscopy (Leica MZ-APO; Leica Microsystems) and scanning electron microscopy (SEM) (Zeiss EVO 50; Carl Zeiss Microscopy LLC) to characterize the failures into 4 patterns: I, crack propagates within the cement layer; II, crack propagates between the cement and ceramic at the same interface; III, crack starts at one interface and goes to the other across the cement thickness; and IV, crack kinks between the 2 interfaces.

Crystalline Phase Assembly

Zirconia phase assembly was characterized using X-ray diffraction (XRD) (X'pertPowder; PANalytical) with nickel-filtered Cu $K\alpha$ radiation, operating at 45 kV and 40 mA. Scans were performed over the 2θ range of 25° to 80° at a scan rate

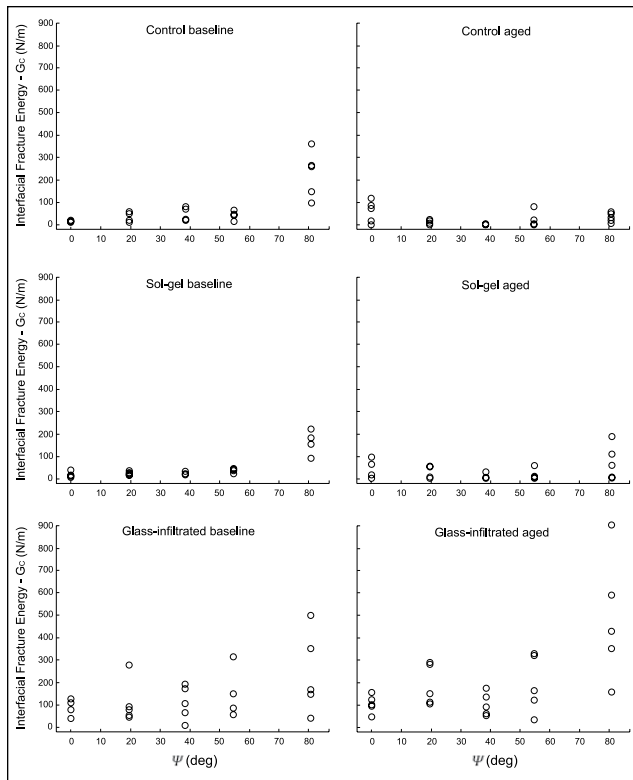


Figure 2. Plots of interfacial fracture energy (G_c) values calculated as a function of loading phase (Ψ), where $\Psi = 0$ represents specimens fractured in mode I (pure tensile) and increasing values of Ψ represent increasing levels of shear (mode II).

of 0.2°/min and a step size of 0.02°. Quantitative phase analysis was carried out using the Rietveld refinement method in X’Pert HighScore software (PANalytical), which estimates the weight fraction (wt.%) of each zirconia phase based on relative peak intensity.

Statistical Analyses

The interfacial fracture energy (G_c) data, according to stress type at the interface (pure tension $\Theta = 0^\circ$ and predominantly shear $\Theta = 25^\circ$), followed a normal distribution ($p_{0^\circ} = 0.585$ and $p_{25^\circ} = 0.209$) and were homoscedastic ($p_{0^\circ} = 0.096$ and $p_{25^\circ} = 0.062$). Thus, a 2-way analysis of variance (ANOVA) general linear model for parametric data was conducted, with factors of surface treatment (control, sol-gel, and glass infiltration) and time (baseline and aged). A post hoc Tukey test was used for all pairwise multiple comparisons. A 5% significance level was set, with a power of analysis greater than 80%.

Results

The fracture load data were analyzed using MATLAB software (MathWorks) and plotted in graphs representing the interfacial fracture energy (G_c , N/m; Fig. 2) for the corresponding loading phase (ψ). In general, for all groups, mode I ($\psi = 0$) tensile

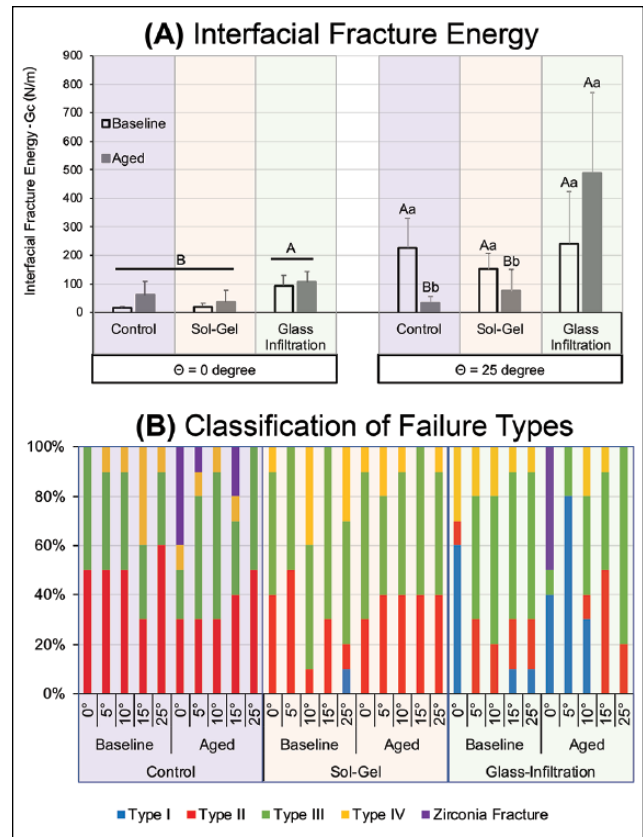


Figure 3. Interfacial fracture test results: (A) Average interfacial fracture energy under pure tension ($\Theta = 0^\circ$) and predominantly shear ($\Theta = 25^\circ$) for each surface treatment and time. Uppercase letters indicate statistical differences among surface treatments, within stress type (Θ). Lowercase letters indicate statistical differences between baseline and aging within surface treatment and stress type. (B) Classification of failure type distribution in each test condition.

stresses at the interface resulted in poorer interfacial fracture energy, whereas increasing shear stresses (mixed modes I and II) denoted a trend in increasing interfacial fracture energy.

Figure 3A shows the analysis of the interfacial fracture energy for each surface treatment when subjected to pure tension $\Theta = 0^\circ$ or predominantly shear $\Theta = 25^\circ$. Under pure tensile stresses (mode I), only surface treatment had a significant effect on G_c ($P < 0.001$). Glass infiltration yielded a higher fracture energy compared to the other 2 groups ($P < 0.002$), which were similar ($P = 0.804$). A distinct behavior was observed when samples were fractured under predominantly shear stresses (mode II): the 2 testing parameters, surface treatment ($P = 0.005$) and time ($P = 0.018$), as well as their interaction ($P = 0.005$), were significant. At baseline, all 3 surface treatments yielded a similar interfacial fracture energy ($P > 0.811$). Aging caused a significant decrease in interfacial fracture energy for the control ($P = 0.002$) and sol-gel ($P = 0.024$) groups but did not affect the glass-infiltrated group ($P = 0.152$), which presented the best results under shear stresses after aging ($P < 0.001$).

The classification of failure type according to surface treatment, angle, and aging is presented in Figure 3B. Failure I,

where the crack propagates within the cement layer, was predominant in the glass-infiltrated group, occurring most often under tensile stresses. A few specimens displayed zirconia fracture, and thus failure mode could not be classified. For these specimens, the maximum load at interfacial fracture was identified by the first load drop registered in the load versus displacement curve. The load at the interfacial fracture could not be identified for only 2 specimens from the aged control group; thus, the specimens were excluded from the study. The 4 failure patterns are illustrated in the SEM images in Figure 4A. The silica infiltration was not uniform in the sol-gel group (Fig. 4B), as observed in the high-magnification SEM image, which depicts silica islands where residual cement is still bonded after fracture.

XRD spectra are shown in Figure 5. Quantifications using the Rietveld refinement method elucidate that both silica-based infiltrations prevented significant zirconia phase transformations, yet sol-gel presents traces of the monoclinic phase (below the detection limit of the equipment). The control group showed a 6% increase in monoclinic content after aging.

Discussion

In this experiment, we have evaluated the interfacial fracture toughness of the adhesively bonded zirconia from the viewpoint of linear elastic fracture mechanics, using the Brazil nut technique. Glass infiltration on the surface of zirconia resulted in higher interfacial toughness compared to air abraded and sol-gel-silica-infiltrated zirconias. In addition, a protective effect against low-temperature degradation was observed for both infiltration techniques.

The sol-gel infiltration used herein is similar to that described by Campos et al. (2016). However, a catalyst was used in this study to decrease the infiltration time and to facilitate the use of this technique in dental laboratories. In a previous study, we observed the formation of multilayers when the

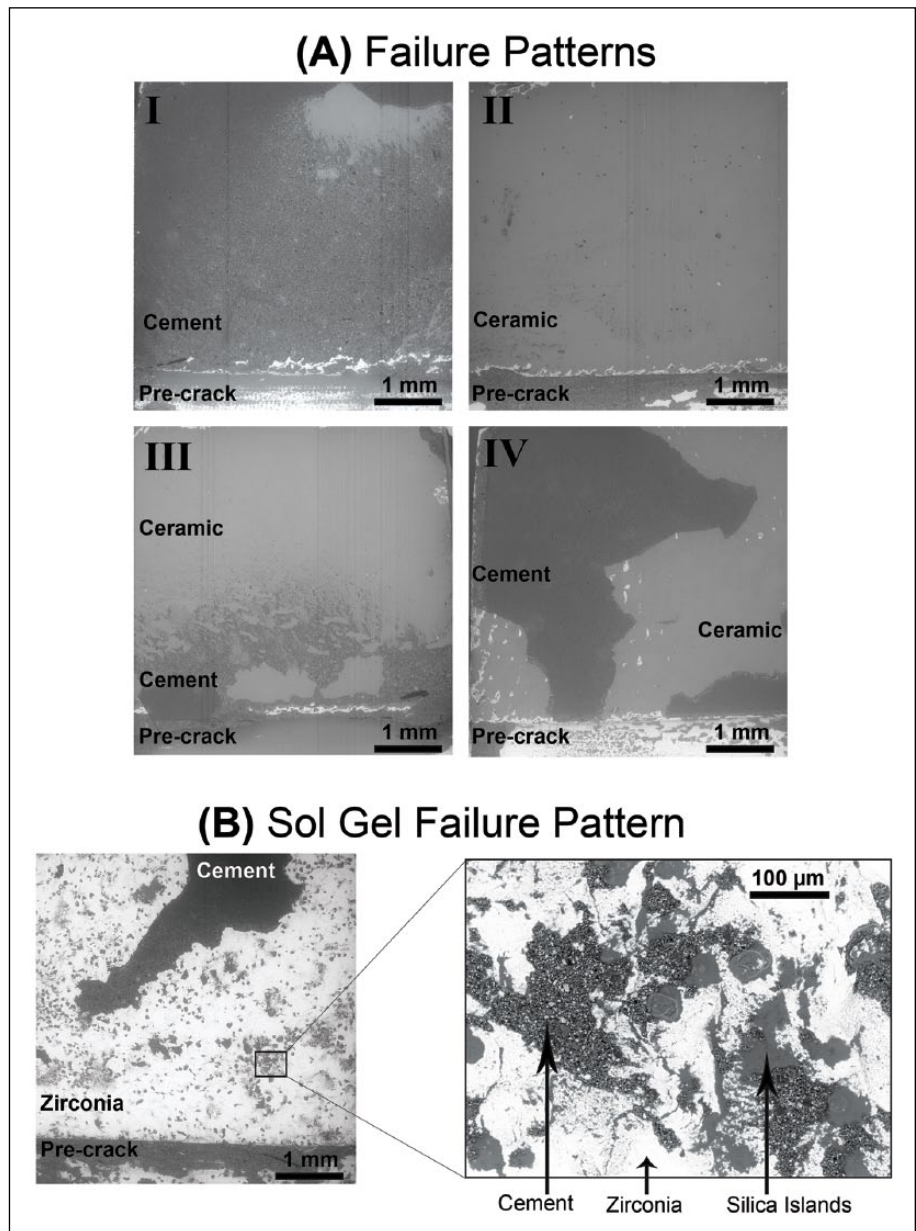


Figure 4. SEM images of intaglio surfaces after interfacial fracture: **(A)** Illustration of the failure modes as classified in this study: I, crack propagates within the cement layer; II, crack propagates between the cement and ceramic at the same interface; III, crack starts at one interface and goes to the other across the cement thickness; and IV, crack kinks between the 2 interfaces. **(B)** For the sol-gel silica infiltration, the coating was not uniform. The high-magnification image shows silica islands where residual cement is still bonded after fracture.

infiltration was performed with the aid of catalysts and repeated twice consecutively (data not yet published). The twice-infiltrated sol-gel groups presented better results for flexural strength and better structural homogeneity, indicated by the greater Weibull modulus, compared to the once-infiltrated sol-gel group and compared to the results of Campos et al. (2016). The amount of silica infiltrated in that group was likely greater, which resulted in filling defects within the ceramic, leading to increases in mechanical properties and structural reliability. On

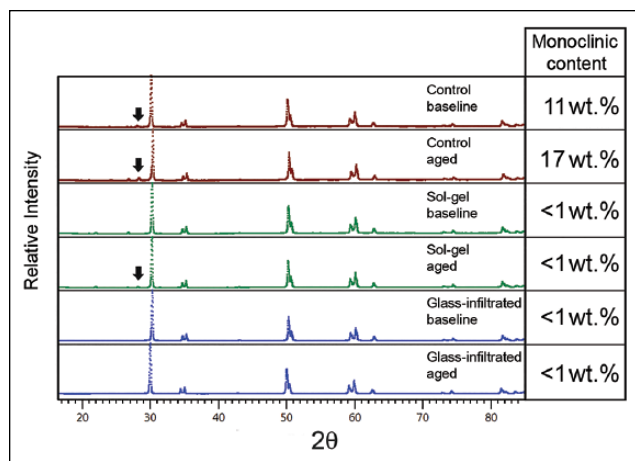


Figure 5. X-ray diffraction spectra for each group, with arrows pointing to the main monoclinic peak in the control and sol-gel groups after aging. Side panels show the monoclinic phase fraction (wt.%) calculated by the Rietveld refinement method.

the other hand, in the present study, as seen in the SEM images (Fig. 4B), the infiltration was not uniform. It is possible to observe silica clusters on the zirconia surface where the resin cement remains bonded. This uneven surface infiltration is possibly related to the minimum phase transformation observed. Thus, we hypothesize that had the infiltration been more homogeneous, the interfacial fracture toughness would have been much improved, which warrants further investigation.

The performance of sol-gel-infiltrated zirconia was not as superior as the glass-infiltrated zirconia but was similar to the control zirconia that was air abraded with aluminum oxide. Surface treatment with air abrasion is controversial in the literature, but some studies show that this bonding is long lasting (Yang et al. 2010; Roselino et al. 2013; Kern et al. 2017).

Usually, to evaluate the susceptibility of interfacial failure, shear tests or tensile tests are used. However, these pure tensile or pure shear tests do not simulate the complex loading scenario in occlusal function (Kelly 1999). Interfacial fracture mechanisms provide a framework that can be used to assess the structural integrity of interfaces that are relevant in dental restorations. In this study, Brazil nut specimens were used to determine interfacial fracture toughness between pure mode I (tensile) and predominantly mode II (shear) failure. The mode I interfacial fracture energy measure herein is similar to that reported in Chai et al. (2015) for control zirconia and glass-infiltrated zirconia. As material fractures are always related to crack initiation/propagation, interfacial fracture toughness values are useful to determine the mechanical behavior of the material and to predict its clinical performance. The Brazil nut specimens, aside from measuring interfacial fracture toughness through the complete range of the failure modes, also have a standard notch that serves as the initial point of the crack growth. The elliptical notch in the center of a Brazil nut specimen was precisely machined in this study, ensuring the accuracy and reliability of this test method.

For most materials, except for some adhesives, fracture toughness increases as the mode-mixity increases. In this study, this trend of behavior was observed for all groups and conditions, except for the control group after aging. This increase as a function of mode-mixity is mainly attributed to the presence of surface forces that inhibit the sliding of the surface cracks (Rahbar et al. 2010).

Generally, the interfacial fracture energy values are much higher than bond-strength values reported in adhesion studies. Zhou et al. (2006) explained that additional energy is required for plastic deformation and the damage of the materials that are close to the interface. The classification of failure types observed in this study corroborated the findings of the mechanical test; failure type I (inside the cement) was predominant in the glass-infiltrated group, for which the interfacial fracture energy was far superior to other groups. Therefore, the toughness of the cement was lower than the toughness of the MDP-bonded ceramic-cement interface, causing cohesive failures of the resin cement. In the sol-gel and control groups, mainly adhesive failures were observed (through the zirconia-cement interface) across the range of mode-mixities. Clinically, glass-infiltrated crowns would hardly debond at the interface unless high shearing stresses could break the cement layer, whereas any stresses would break the cement-ceramic interfaces of conventionally bonded and silica-infiltrated zirconia crowns after a certain time in service.

After aging, there were even more cohesive failure patterns shown in the GI group. Similar behavior was reported by Quaas et al. (2007), where the water storage after 150 d decreased the cohesive strength of the Panavia F 2.0. In this particular study, resin cement degradation due to the hydrolysis of the bonds between the resin matrix and the silanated fillers was observed. The mechanical properties of the resin cement used as well as the cement thickness at the interface are other parameters that need to be further investigated.

Conclusions

According to the results, the following can be concluded:

- Glass infiltration of the zirconia intaglio surface bonded with an MDP-based resin cement yields robust and stable bonding.
- The technique for zirconia silica infiltration using the sol-gel method requires improvement to obtain homogeneous surface infiltration and enhanced bondability.
- Aging reduces the interfacial fracture energy of poorly bonded zirconia in both control and sol-gel groups.


Author Contributions


N.C. Ramos, M.R. Kaizer, Y. Zhang, R.M. Melo, contributed to conception, design, and data analysis, drafted and critically revised the manuscript; T.M.B. Campos, contributed to conception, design, and data analysis, drafted the manuscript; J. Kim, contributed to data analysis, critically revised the manuscript. All authors gave final approval and agree to be accountable for all aspects of the work.

Acknowledgments

The authors thank Prof. Do Kyung Kim for valuable help on XRD phase analysis and Dr. Minglei Zhao for assistance in ceramic sintering. Funding was provided by National Institutes of Health/National Institute of Dental and Craniofacial Research (grants R01DE026772, R01DE026279, and R01DE017925) and FAPESP–São Paulo State Foundation (grants 2015/16387-7, 2016/20001-0, and 2016/07920-6). The authors declare no potential conflicts of interest with respect to the authorship and/or publication of this article.

ORCID iDs

N.C. Ramos  <https://orcid.org/0000-0002-0977-5350>

M.R. Kaizer  <https://orcid.org/0000-0002-6308-6089>

Y. Zhang  <https://orcid.org/0000-0002-6738-3769>

References

- Atkinson C, Smelser RE, Sanchez J. 1982. Combined mode fracture via the cracked Brazilian disc test. *Int J Fract.* 18(4):279–291.
- Brinker CJ. 1988. Hydrolysis and condensation of silicates: effects on structure. *J Non-Cryst Solids.* 100(1–3):31–50.
- Campos TM, Ramos NC, Machado JP, Bottino MA, Souza RO, Melo RM. 2016. A new silica-infiltrated Y-TZP obtained by the sol-gel method. *J Dent.* 48:55–61.
- Chai H, Kaizer M, Chughtai A, Tong H, Tanaka C, Zhang Y. 2015. On the interfacial fracture resistance of resin-bonded zirconia and glass-infiltrated graded zirconia. *Dent Mater.* 31(11):1304–1311.
- Chevalier J, Gremillard L, Virkar AV, Clarke DR. 2009. The tetragonal-monoclinic transformation in zirconia: lessons learned and future trends. *J Am Ceram Soc.* 92(9):1901–1920.
- Kaizer MR, Almeida JR, Goncalves APR, Zhang Y, Cava SS, Moraes RR. 2016. Silica coating of nonsilicate nanoparticles for resin-based composite materials. *J Dent Res.* 95(12):1394–1400.
- Kelly JR. 1999. Clinically relevant approach to failure testing of all-ceramic restorations. *J Prosthet Dent.* 81(6):652–661.
- Kern M. 2015. Bonding to oxide ceramics-laboratory testing versus clinical outcome. *Dent Mater.* 31(1):8–14.
- Kern M, Passia N, Sasse M, Yazigi C. 2017. Ten-year outcome of zirconia ceramic cantilever resin-bonded fixed dental prostheses and the influence of the reasons for missing incisors. *J Dent.* 65:51–55.
- Kim JW, Liu L, Zhang Y. 2010. Improving the resistance to sliding contact damage of zirconia using elastic gradients. *J Biomed Mater Res B Appl Biomater.* 94(2):347–352.
- Melo RM, Rahbar N, Soboyejo W. 2011. Interfacial fracture of dentin adhesively bonded to quartz-fiber reinforced composite. *Mat Sci Eng C-Mater.* 31(4):770–774.
- Mesmar S, Ruse ND. 2017. Interfacial fracture toughness of adhesive resin cement-lithium-disilicate/resin-composite blocks. *J Prosthodont* [epub ahead of print 15 Sep 2017]. doi:10.1111/jopr.12672
- Oliveira-Ogliari A, Collares FM, Feitosa VP, Sauro S, Ogliari FA, Moraes RR. 2015. Methacrylate bonding to zirconia by in situ silica nanoparticle surface deposition. *Dent Mater.* 31(1):68–76.
- Quaas AC, Yang B, Kern M. 2007. Panavia F 2.0 bonding to contaminated zirconia ceramic after different cleaning procedures. *Dent Mater.* 23(4):506–512.
- Rahbar N, Jorjani M, Riccardelli C, Wheeler G, Yakub I, Tan T, Soboyejo WO. 2010. Mixed mode fracture of marble/adhesive interfaces. *Mat Sci Eng A Struct.* 527(18–19):4939–4946.
- Roselino Lde M, Cruvinel DR, Chinelatti MA, Pires-de-Souza Fde C. 2013. Effect of brushing and accelerated ageing on color stability and surface roughness of composites. *J Dent.* 41(Suppl 5):e54–e61.
- Samodurova A, Kocjan A, Swain MV, Kosmač T. 2015. The combined effect of alumina and silica co-doping on the ageing resistance of 3Y-TZP bioceramics. *Acta Biomater.* 11:477–487.
- Tanaka R, Fujishima A, Shibata Y, Manabe A, Miyazaki T. 2008. Cooperation of phosphate monomer and silica modification on zirconia. *J Dent Res.* 87(7):666–670.
- Toyama DY, Alves LMM, Ramos GF, de Campos TMB, de Vasconcelos G, Borges ALS, Melo RM. 2019. Bioinspired silica-infiltrated zirconia bilayers: strength and interfacial bonding. *J Mech Behav Biomed Mater.* 89:143–149.
- Vanderlei A, Bottino MA, Valandro LF. 2014. Evaluation of resin bond strength to yttria-stabilized tetragonal zirconia and framework marginal fit: comparison of different surface conditionings. *Oper Dent.* 39(1):50–63.
- Wang J, Suo Z. 1990. Experimental-determination of interfacial toughness curves using Brazil-nut-sandwiches. *Acta Metall Mater.* 38(7):1279–1290.
- Yang B, Barloi A, Kern M. 2010. Influence of air-abrasion on zirconia ceramic bonding using an adhesive composite resin. *Dent Mater.* 26(1):44–50.
- Zhang Y. 2012. Overview: damage resistance of graded ceramic restorative materials. *J Eur Ceram Soc.* 32(11):2623–2632.
- Zhang Y, Chai H, Lee JJ, Lawn BR. 2012. Chipping resistance of graded zirconia ceramics for dental crowns. *J Dent Res.* 91(3):311–315.
- Zhang Y, Kim JW. 2009. Graded structures for damage resistant and aesthetic all-ceramic restorations. *Dent Mater.* 25(6):781–790.
- Zhang Y, Kim JW. 2010. Graded zirconia glass for resistance to veneer fracture. *J Dent Res.* 89(10):1057–1062.
- Zhang Y, Ma L. 2009. Optimization of ceramic strength using elastic gradients. *Acta Mater.* 57(9):2721–2729.
- Zhou J, Huang M, Sagnang F, Soboyejo WO. 2006. Interfacial failure of a dental cement composite bonded to glass substrates. *Dent Mater.* 22(6):585–591.